Laser-Induced Incandescence Study on the Metal Aerosol Particles as the Effect of the Surrounding Gas Medium

Yoshinori Murakami,* Tsuyoshi Sugatani, and Yoshio Nosaka

Department of Chemistry, Nagaoka University of Technology, Nagaoka, Niigata 940-2188, Japan

Received: February 8, 2005

The fundamental heat transfer phenomena caused by the 1064 nm pulsed laser irradiations on the molybdenum aerosol particles were investigated by monitoring the time evolutions of the incandescence spectra using an ICCD detector with a multichannel spectrograph. The particle temperatures were evaluated from the incandescence spectra with the Planck function, and the cooling processes of the laser-heated particles were investigated. By measuring the decrease in the laser-heated particle temperatures with different surrounding media, the roles of the heat transfer processes such as vaporization, thermal radiation, and heat conduction to the surrounding media were discussed. The influences of the vaporization processes on the total heat transfer phenomena were investigated by monitoring the emissions of the constituent molybdenum atoms in the laser-induced incandescence spectra of the aerosol particles and also by investigating the relationships between the intensity of the incandescence and the fluence of the 1064 nm pulsed laser. The calculations using the theory of heat conduction suggested that the diameters of the particles produced by the photolysis of $Mo(CO)_6$ depended on the nature of the surrounding gases.

Introduction

Recently, it has been recognized that small metal and semiconductor particles have different electronic and optical properties from their bulk counterparts. For example, Chen et al.[1] observed a transition from metal-like double-layer capacitive charging to redox-like charging on solutions of gold nanoparticles of various core sizes. Li et al.[2] also observed the band gap variations of size- and shape-controlled colloidal CdSe quantum rods. For those size dependent electronic and optical properties, considerable attempts have been made in controlling the size distributions of the metal and semiconductor particles. Therefore, a lot of experimental efforts have been devoted to controlling the size distributions of the particles by buildup processes such as the nucleation processes, but few studies have been carried out on the breaking-down processes by reducing the sizes. Recently, Takami et al.[3] reported that the pulsed laser irradiations to the silver particles in aqueous solution could reduce the sizes of the particles and proposed that this laser-induced size reduction could be used as a new technique to control the size distributions with the breaking-down process. They also investigated the size reductions of the gold particles in aqueous solution under pulsed laser irradiations[4,5] and concluded that melting and vaporization of the gold particles under the irradiations of the laser lights caused shape changes and size reductions of the particles. On the other hand, Kamat et al.[6] reported that the 40−60 nm silver clusters broke up into smaller silver clusters (5−20 nm) with 355 nm laser pulse excitations but only larger particles were found to break up with 532 nm laser pulses. They concluded that electron ejections from the silver clusters depended on the choice of the excitation wavelength and such photoejected electrons caused the fragmentations of the silver clusters. However, the mechanism of the laser-induced size reduction is not fully understood yet.

* Corresponding author. Phone: +81-258-47-9329. Fax: +81-258-47-9300. E-mail murakami@chem.nagaokaut.ac.jp.

Since the first discovery of Eckbreth[7] that soot particles heated by pulsed laser lights emitted incandescence in the visible region, the laser-induced incandescence from the soot particles is now often used as the diagnostic tool for detecting the soot in combustion processes. Although the practical applications of the laser-induced incandescence of the soot particles in combustion processes have been reported by several researchers,[8−11] the fundamental heat loss mechanism of the laser-heated soot particles has not been fully understood. Attempts to simulate the temporal decays of the laser-induced incandescence were performed by Melton[12] and later Roth and co-workers[13,14] for developing a new in situ method for the determination of the particle size distributions in a variety of reactors. Recently, Schraml et al.[15] made detailed numerical calculations of the time-resolved laser-induced incandescence and compared the relative magnitudes of the various heat loss paths of the laser-heated soot particles. They concluded that vaporization was the dominant mechanism for some 100 ns and that afterward the conduction determined the temperature decays of the soot particles. On the basis of these theoretical calculations, they claimed that this laser-induced incandescence could be used as a new technique for the simultaneous determination of the size distribution and number density of the particles.

The measurements of laser-induced incandescence are very promising for understanding the heat loss mechanism of metal particles, but up to now, experiments on the laser-induced incandescence of particles other than soot have been very limited. Vander Wal et al.[16] measured the laser-induced incandescence spectra of metal particles produced by the ablations of metal substrates, but a detailed analysis of the heat loss processes of metal particles has not yet been fully discussed.

Because the spectra of the laser-induced incandescence are sensitive to the temperatures of the particles, the spectroscopic studies on the laser-induced incandescence of metal particles will give new insights into the heat transfer processes of metal particles heated by pulsed laser irradiations.

10.1021/jp058044n CCC: $30.25
Published on Web 09/17/2005

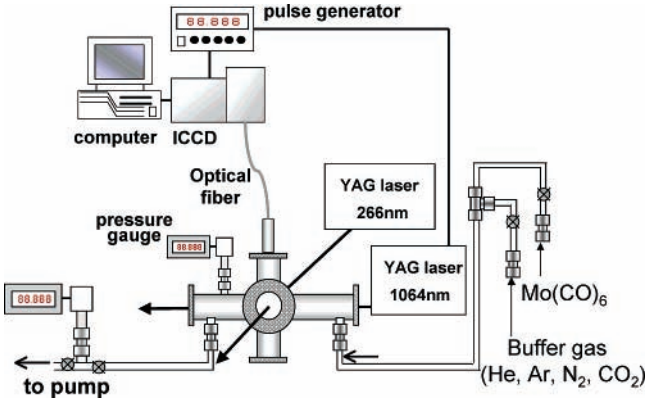

Figure 1. Schematic illustration of the experimental setup.

In this paper, by measuring the incandescence spectra of laser-heated metal particles in several different surrounding media, the roles of vaporization, thermal radiation, and heat conduction were investigated. Attempts to observe the particle vaporization processes were also carried out by monitoring the emissions of the constituent Mo atomic lines from the laser-heated metal particles, and the influences of the laser intensities on the vaporization processes of particles were discussed.

Experimental Section

The apparatus used in the present work is shown schematically in Figure 1. Before each experiment, the reaction cell was pumped down to 10^{-4} Torr (1 Torr = 133.3 Pa). The leakage of the reaction cell from the atmosphere was carefully controlled to be <1 Torr in a day. After 0.1 Torr of $Mo(CO)_6$ diluted with 600 Torr of a buffer gas was introduced through a vacuum line into the reaction cell, the gaseous mixture was irradiated by the fourth harmonic of a pulsed Nd:YAG laser (Continuum Minilite II) at 266 nm with repetition rates of 10 Hz during the experiments. In the present work, He, Ar, N_2, and CO_2 were used for the buffer gases. The aerosol particles formed by the irradiations of the 266 nm laser were irradiated by the fundamental light of a pulsed Nd:YAG laser (Spectron SL-803) at 1064 nm to heat up the aerosol particles in the reaction cell about 1 ms after the 266 nm laser irradiation. The diameters of the 266 and 1064 nm laser beams were 5 mm and 1.0 cm, respectively. Both lasers were not focused and were crossed at the center of the reaction cell perpendicular to each other. The laser-induced incandescence was monitored by a photomultiplier tube (Hamamatsu R106UH) through an interference filter with λ = 400 nm (fwhm = 40 nm) attached to the reaction cell perpendicular to the two laser beams, and the time-resolved signals of the laser-induced incandescence were recorded in a 350 MHz oscilloscope (Lecroy LT262). To measure the spectra of the laser-induced incandescence, an intensified CCD detector (Andor DH501) with a multichannel imaging spectrograph (ORIEL model 77441) was attached to the reaction cell through an optical fiber. The delay and the gate width of the ICCD detector were controlled by a pulse generator (Stanford DG535) triggered by the laser pulse at 1064 nm. The whole spectrum was calibrated by calibrated lamps (Ushio, JC24V150W, JCV100V100WGS).

To confirm that the aerosol particles were formed by the irradiations of 266 nm laser pulses, attempts to collect these particles were performed by placing the substrate just below the 266 nm laser beam in the reaction cell. However, because of the low vapor pressure of $Mo(CO)_6$, it was not possible to collect a great enough amount of the aerosol particles on the substrate to characterize the particles. Therefore, the size distributions and the chemical compositions of the particles have not been analyzed in the present work.

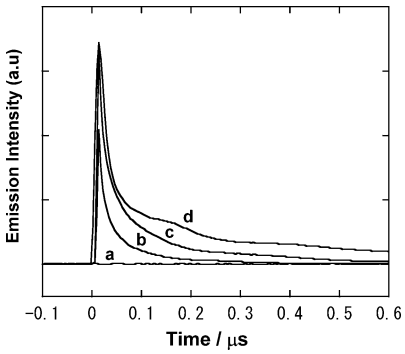

Figure 2. Temporal decays of the laser-induced incandescence monitored around 400 nm (a) before irradiation and after (b) 1 min, (c) 5 min, and (d) 9 min of irradiation of the fourth harmonic of Nd:YAG laser pulses at 266 nm with 3 mJ/pulse at 10 Hz to the gaseous mixture of 0.1 Torr of $Mo(CO)_6$ in 600 Torr of Ar gas. The laser fluence of the fundamental light of the Nd:YAG laser at 1064 nm was 130 mJ/cm^2.

Results and Discussion

Since the particle formations are initiated by the photolysis of $Mo(CO)_6$ at 266 nm and the intensity of the incandescence is proportional to the number of the particles in the reaction cell, the intensity of the incandescence from the laser-heated particles increases with the irradiation time of the fourth harmonic of the Nd:YAG laser at 266 nm. Figure 2 shows a typical example of the time-resolved signals of the incandescence with the irradiations of the 1064 nm laser light, which are monitored by the photomultiplier tube attached to the reaction cell at a wavelength around 400 nm. No incandescence was observed before the irradiations of 266 nm laser light to the gaseous mixtures of 0.1 Torr $Mo(CO)_6$ in 600 Torr of Ar gas. On the other hand, the signals of the incandescence from the laser-heated particles appeared after the irradiations of 266 nm laser light to the reaction cell and the intensities of the laser-induced incandescence increased with increasing irradiation time of the 266 nm laser light.

To clarify further that the signals observed by the photomultiplier tube were the incandescence of the laser-heated particles in the reaction cell, the signals of the laser-induced incandescence were monitored after pumping all of the particles in the reaction cell through the vacuum line. It was found that the incandescence signals disappeared when all of the particles in the reaction cell were pumped down through the vacuum line. It was also found that the signals of the laser-induced incandescence were still observed without any irradiations of 266 nm laser light once the particles were formed in the reaction cell. Therefore, it was concluded that the emissions observed by the photomultiplier tube were the signals of the incandescence from the particles heated by the fundamental light of the Nd:YAG laser at 1064 nm. It was also found that the signal intensities of the laser-induced incandescence were nearly constant even several minutes after the 266 nm laser irradiation had been stopped. These observations indicated that the particles produced by the 266 nm laser photolysis of $Mo(CO)_6$ were uniformly distributed inside the reaction cell and that the signals of the laser-induced incandescence were obtained from the particles that happened to be in the viewing region. As shown in Figure 2, not only was the intensity of the incandescence increased, but also the decay rate became slower with the

irradiation time of the 266 nm laser light. The intensity of the incandescence emitted from a spherical particle surface is given by eq 1

$$I_\lambda = 4\pi a^2 \epsilon e_b(\lambda, T_p) \quad (1)$$

where a is the particle radius, ϵ is the spectral emissivity, and $e_b(\lambda, T_p)$ is the Planck function. Equation 2

$$e_b(\lambda, T_p) = (2hc^2/\lambda^5)/(\exp(hc/\lambda k T_p) - 1) \quad (2)$$

gives the radiation from a blackbody at the temperature T_p and the wavelength λ, where h is the Planck constant and c is the speed of light in a vacuum.[14] The intensity of the incandescence depends inversely on the exponential of the temperature T_p, and therefore, the decays of the incandescence intensity are mainly caused by the temperature decrease of the particles heated by the laser light at 1064 nm.

According to the particle-cooling theory, there are three physical processes that cause the cooling of a particle: heat radiation, heat transfer to the surrounding gas, and particle vaporization.[13−15] Since the total heat flux dq/dt is equal to the sum of all of these heat loss processes mentioned above, the total heat flux from the particle in the free molecular regime is given in the following equations:[13]

$$dq/dt = 4\pi a^2 (^1/_2) p_g c_t (T_p/T_g - 1) + 4\pi a^2 \epsilon \sigma (T_p^4 - T_g^4) + 4\pi a^2 G_v \Delta h \quad (3)$$

$$c_t = (8kT_g/\pi m_g)^{1/2}$$

where p_g is the gas pressure, m_g and c_t are the mass and average thermal velocities of the gas molecules, ϵ is the total emissivity coefficient, k and σ are the Bolzmann and Stefan−Bolzmann constants, G_v is the flux density of the vapor leaving the particle, and Δh is the specific heat of vaporization. The first term on the right-hand side of the equation describes the heat conductivity, the second term describes the particle heat radiation, and the last term accounts for the cooling process due to the vaporization process. Since the second and last terms corresponding to the heat radiation and vaporization processes are smaller in comparison with the first term corresponding to the heat transfer process to the surrounding gas, eq 3 can be simplified to become

$$dq/dt = 4\pi a^2 (^1/_2) p_g c_t (T_p/T_g - 1) \quad (4)$$

Because of the requirements of the energy balance between the heat flux and the particle internal energy, the following equation holds assuming the particle temperature T_p inside the particle is uniform

$$dq/dt = -m_p C_p (dT_p/dt) \quad (5)$$

Equation 4 together with eq 5 can be easily integrated, and the solution of the temporal decays of the particle temperature T_p can be obtained.

$$(T_p - T_g)/T_g = (T_p^0/T_g - 1) \exp(-t/\tau) \quad (6)$$

$$\tau = 2aC_p\rho_p T_g / 3c_t p_g \quad (7)$$

where T_p^0 is the particle temperature at $t = 0$. The parameter τ represents the characteristic cooling time of the particle. According to eq 7, the cooling rate of the particle becomes slower when the particle radius becomes larger. That is, the observations that the decay rates of the laser-induced incandescence decreased with an increase in the irradiation time of the 266 nm laser light can be explained by the decrease in the particle-cooling rate because of the increase in the particle radius. However, these conclusions were only derived from the theories of the heat transfer phenomena based on several assumptions and more direct experimental evidence for understanding the roles of the three different particle-cooling processes was desired. Therefore, the temporal decays of the particle temperatures in several different surrounding media were measured by monitoring the incandescence spectra of the laser-heated particles and the roles of the three physical processes, that is, heat radiation, heat transfer to the surrounding gas, and particle vaporization, were investigated. It was anticipated that the rate of heat transfer to the surrounding media depended on the surrounding gases used, while the heat loss of the particles by the vaporization process was independent of the surrounding gases.

Before measuring the temporal decays of the particle temperatures using the incandescence spectra, the dependence of the incandescence intensity on the fluence of the pulsed laser irradiation at 1064 nm in several different surrounding media was investigated. The incandescence intensity is defined as the maximum incandescence intensity determined by the temporal profiles of the laser-induced incandescence signals obtained by the photomultiplier tube. As shown in Figure 3, in the case of N_2 and CO_2, the incandescence signals increased with increasing laser fluence up to 150 mJ/cm^2 but the intensities of the laser-induced incandescence became constant thereafter. On the other hand, in the case of He and Ar, the incandescence signals increased slowly with increasing laser fluence up to 250 mJ/cm^2 and then the intensities of the laser-induced incandescence began to decrease with increasing laser fluence at 1064 nm. Vander Wal et al.[18] also investigated the relationships between the transmitted laser energy and the signal intensity of the laser-induced incandescence of the soot particles. They found that the transmitted laser energy rapidly increased when the signal intensities of the laser-induced incandescence decreased due to the increase in laser energy. They also observed the formation of hollow shells in the laser-heated soot particles by an electron microscopy technique.[19] For these observations, they concluded that the decrease in the laser-induced incandescence signals was attributed to the morphological changes of the soot particles because of the high laser fluence. Since the incandescence intensity depends on both the particle temperature and size, as shown by eq 1, the vaporization process of the aerosol particles at the high laser fluence decreases the particle size and causes a decrease in the incandescence intensity. Our observations that the intensities of the laser-induced incandescence began to decrease with increasing laser fluence at 1064 nm might be due to such vaporization effects. Since the saturations of the excitation processes can also cause such nonlinear dependence of the incandescence intensity versus the laser fluence, the saturation effects might be the reason for such dependence. Further detailed analysis is necessary for understanding the reasons of such dependences, but in the present work to avoid such complications arising from the particle vaporizations and the saturation effects of the excitation laser pulses, the measurements of the particle temperatures using the incandescence spectra were performed at 130 mJ/cm^2 in the case of N_2 and CO_2 and at 200 mJ/cm^2 in the case of He and Ar.

Figure 4 shows a typical example of the incandescence spectra obtained with various delay times between the measurement of

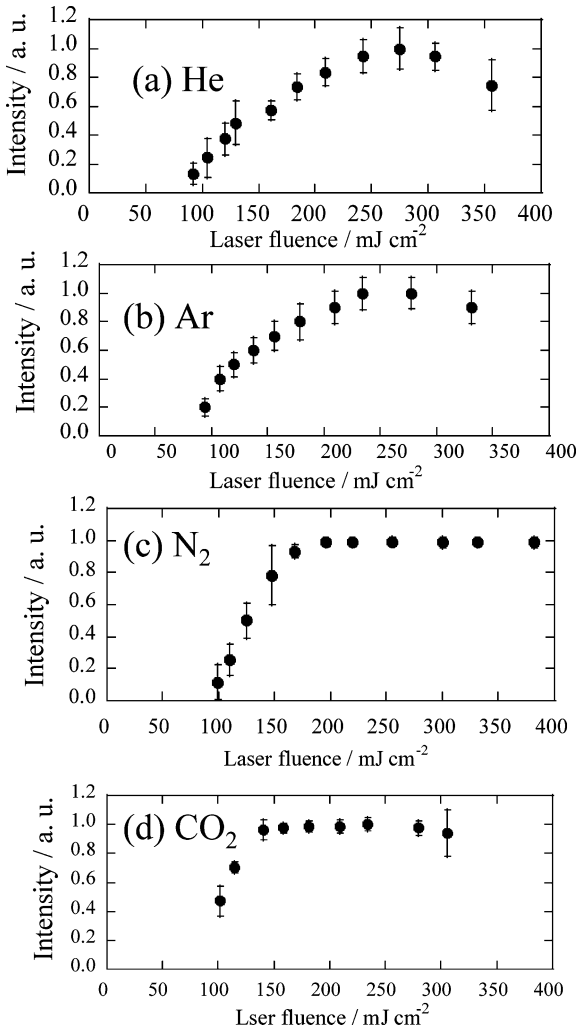

Figure 3. Relationship between the intensity of the laser-induced incandescence and the laser fluence of the fundamental light of the Nd:YAG laser at 1064 nm. The gaseous mixtures irradiated by the 266 nm laser are 0.1 Torr of $Mo(CO)_6$ in 600 Torr of (a) He, (b) Ar, (c) N_2, and (d) CO_2 gas.

the spectrum and the irradiation of the 1064 nm laser. The intensities and decay rates of the incandescence obtained by the pulsed irradiation of the 1064 nm laser changed with the irradiation time of the 266 nm laser light because of the particle growth in the reaction cell, as mentioned above. Then, the spectra were taken after the 266 nm laser light irradiations of more than 30 min, when the stationary conditions of the particle formation in the reaction cell were attained. It was confirmed that the signal intensities and decay rates measured by the photomultiplier tube were almost unchanged after 30 min of irradiation with the 266 nm laser light. As shown in Figure 4, the incandescence spectra were shifted from the visible region to the near-infrared region with an increase in the delay times between the measurement and the 1064 nm pulsed laser irradiation. Since the spectral shift from the visible region to the near-infrared region corresponds to a decrease in the particle temperature, the experimental results in Figure 4 indicate the cooling processes of the particles heated by the pulsed laser irradiation at 1064 nm. To transform the incandescence spectra to the particle temperatures, these spectra were fitted with the Planck function (eq 2) assuming that the emissivity of the particle was unity for all of the wavelength regions measured in the incandescence spectra as was defined in a blackbody radiation. To not confuse the real particle temperature with the

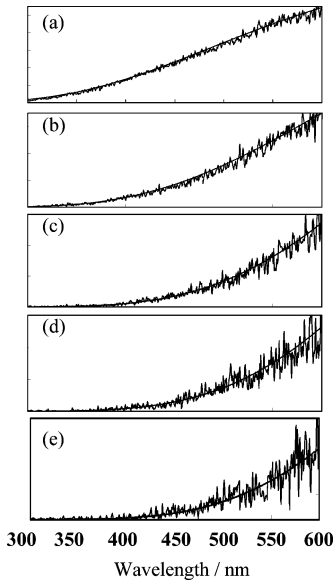

Figure 4. Laser-induced incandescence spectra of the laser-heated aerosol particles formed by the irradiations of the fourth harmonic of the Nd:YAG laser at 266 nm to the gaseous mixtures of 0.1 Torr of $Mo(CO)_6$ in 600 Torr of CO_2 gas. Each part corresponds to different delay times of (a) 50 ns, (b) 550 ns, (c) 1250 ns, (d) 1750 ns, and (e) 2250 ns between the measurement. For heating the aerosol particles in the reaction cell, pulsed irradiations of the fundamental light at 1064 nm with a fluence of 130 mJ/cm^2 were employed. The solid lines are the Plank functions fitted with (a) 3500 K, (b) 2800 K, (c) 2300 K, (d) 2200 K, and (e) 2100 K.

particle temperature determined by fitting with the Planck function, we will call these calculated particle temperatures the "apparent particle temperatures" hereafter. The fits to the experimental spectra were also shown by the solid lines in Figure 4. As shown in Figure 4, a reasonable fit was obtained for each spectrum with different delay times.

Figure 5 shows a summary of the results for the particle-cooling processes with various surrounding gases. As shown in Figure 5, the maximum temperatures of the laser-heated particles varied with different surrounding media. Therefore, to make the comparisons easier, the temporal decays of the apparent particle temperatures were normalized with the maximum temperature of each surrounding medium. As shown in Figure 6, the cooling rates of the particles were almost the same between the different surrounding gases (He, Ar, N_2, and CO_2) within 0.4 μs after the pulsed 1064 nm laser irradiations. Furthermore, the rates of the heat loss process within 0.4 μs after the pulsed 1064 nm laser irradiations were about 1500 K/μs, which are more than 3 times larger than the rates of the particle-cooling processes about 0.4 μs after the pulsed 1064 nm laser irradiations. On the other hand, about 0.4 μs after the pulsed 1064 nm laser irradiations, the rates of the particle-cooling processes depended on the surrounding gases, as shown in Figure 6. That is, the rates of the particle-cooling process are larger in CO_2 and N_2 and smaller in He and Ar. This is consistent with the heat transfer theory that the heat conduction is proportional to the number of internal degrees of freedoms such as vibrations and rotations in the surrounding gas. Since CO_2 and N_2 have vibrational and rotational degrees of freedoms and He and Ar do not, the rates of heat transfer in CO_2 and N_2 are much more larger than those in He and Ar. Thus, the cooling rates in Figure 6 are well explained. On the other hand, up to 0.4 μs, there were no differences in the rates of the particle-cooling processes between the surrounding gases, as shown in Figure 6. Since the vaporization processes of the particles have

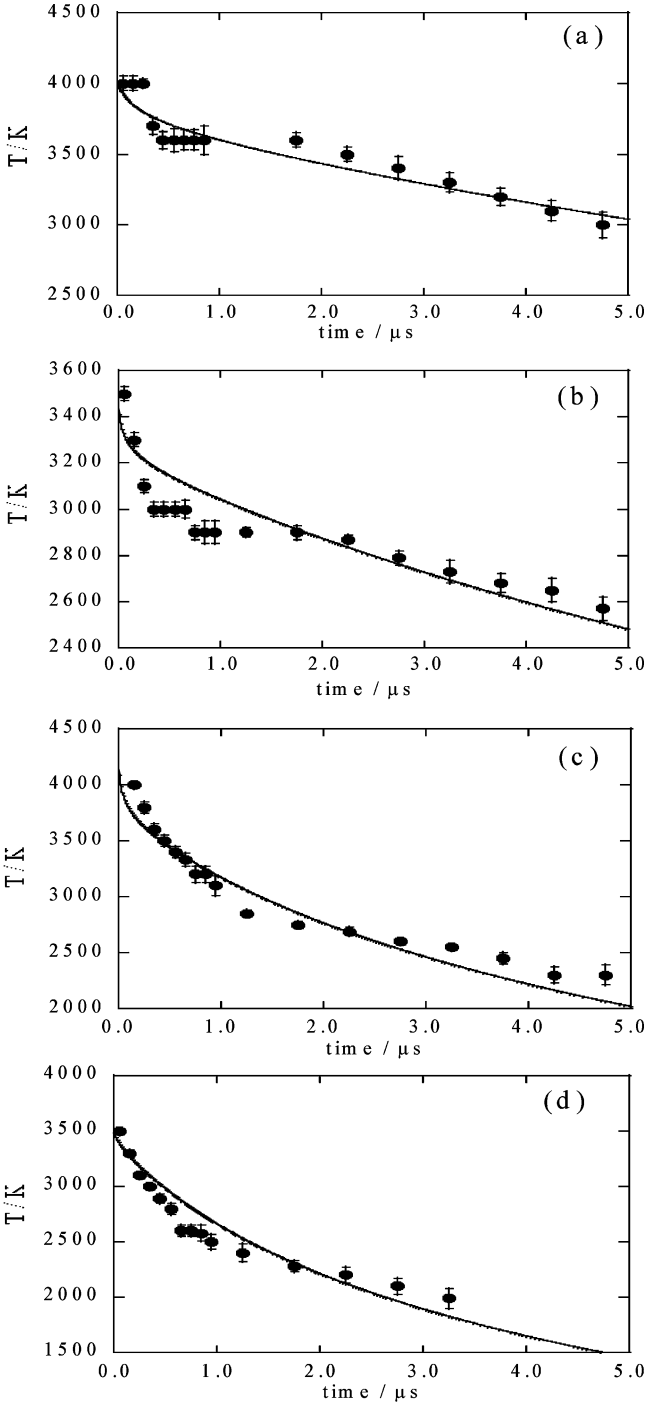

Figure 5. Time evolutions of the aerosol particle temperatures heated by the fundamental light of the Nd:YAG laser at 1064 nm with different surrounding gases: (a) He; (b) Ar; (c) N_2; (d) CO_2. The pulsed laser irradiation of the fundamental light at 1064 nm was 200 mJ/cm^2 in He and Ar and 130 mJ/cm^2 in N_2 and CO_2. The solid lines are simulated temporal decays of the aerosol particle temperatures in eq 3.

no or little influence on the surrounding gases, it is reasonable to conclude that the main cooling process up to 0.4 μs is the vaporization process but not the heat transfer to the surrounding gas.

According to eqs 6 and 7, the mean particle diameters of the particles can be determined by fitting the temporal decays of the apparent particle temperatures. Since the temporal decays of the apparent particle temperatures consisted of the fast and slow components, as shown in Figure 6, and the fast components corresponded to the vaporization processes, only the slow components were analyzed to evaluate the corresponding particle diameters. The plots of $\ln((T_p - T_g)/T_g)$ versus time in various media were summarized in Figure 7. As shown in Figure 7, the linear relationships were obtained in the plots of $\ln((T_p - T_g)/T_g)$ versus time for each surrounding media. From these slopes and the atomic and molecular parameters of the surrounding gases, the particle diameter for each surrounding medium was calculated. For calculating the particle diameters using eqs 6 and 7, it is necessary to know the particle density ρ_p and the specific heat capacity C_p of the particle material. Because the characterization of the aerosol particles produced by the irradiations of the 266 nm laser light was unsuccessful, as mentioned in the Experimental Section, the particle density ρ_p and the specific heat capacity C_p of the particle material were supposed to be the same values as those for the molybdenum particles, which are 10 220 kg m^{-3} and 250 J kg^{-1} K^{-1}, respectively. The results were summarized in Table 1. As shown in Table 1, the particle diameters are larger in He and Ar but smaller in N_2 and CO_2. These relationships hold without any assumptions of the particle density and the specific heat capacity of the particles.

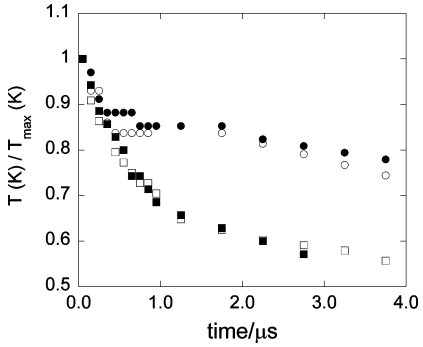

Figure 6. Time evolutions of the normalized aerosol particle temperatures heated by the fundamental light of the Nd:YAG laser at 1064 nm with different surrounding gases: (○) He; (●) Ar; (□) N_2, (■) CO_2.

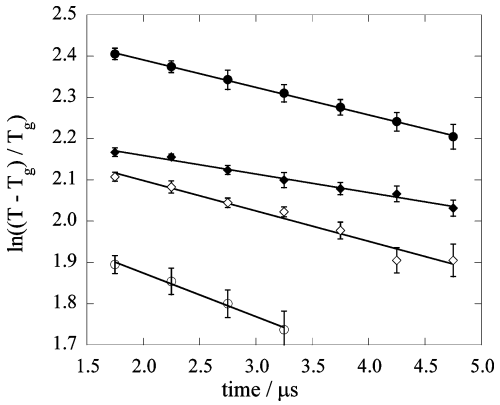

Figure 7. Plots of $\ln((T_p - T_g)/T_g)$ versus time with different surrounding gases: (●) He; (◆) Ar; (◇) N_2; (○) CO_2. The solid lines are the least-squares fits for each surrounding gas.

TABLE 1: Summary of the Characteristic Particle-Cooling Times and the Predicted Particle Diameters in Various Surrounding Gases

	atomic or molecular weight	thermal velocity (c_t), m s^{-1}	characteristic cooling time (τ), μs	particle diameter (a), μm
He	4.003	1255.8	15.0 ± 0.5	3.0 ± 0.1
Ar	39.95	397.1	22.2 ± 3.0	1.4 ± 0.2
N_2	28.02	474.5	13.6 ± 3.0	1.0 ± 0.2
CO_2	44.01	379.0	9.5 ± 1.7	0.6 ± 0.1

It is well-known in the unimolecular reaction theories that the recombination reactions of free radicals such as

$$R\bullet + R\bullet + M \rightarrow R{-}R + M \quad (8)$$

show some pressure dependence on the surrounding gas and in many cases the rate constants of these recombination reactions are also dependent on the nature of the surrounding gas.[20] According to the unimolecular reaction theories, the surrounding gas acts as the acceptor of energies released by the recombination reaction of free radicals and therefore the rate constant for the recombination reaction is greater when the molecule of the surrounding gas has more accepting modes of freedoms. Our experimental results that the particle diameters are larger in He and Ar but not in N_2 and CO_2 are consistent with such energy acceptor models of the radical recombination processes because N_2 and CO_2 have much more accepting modes such as the vibrational and rotational modes. That is, the surrounding gases such as He, Ar, N_2, and CO_2 might also act as the energy acceptors in the particle growths from the small clusters.

Since the mean particle diameters of the particles were determined by the linear relationships in the plots of $\ln((T_p - T_g)/T_g)$ versus time for each surrounding medium, it is now possible to evaluate the contributions of each heat loss process, that is, heat radiation, heat transfer to the surrounding gas, and particle vaporization, using eq 3. According to Melton,[12] the flux density of vapor G_v in eq 3 is given by the products of the density of the vaporized gas ρ_v and the vapor velocity U_v:

$$G_v = \rho_v U_v \quad (9)$$

We also assumed that the vapor velocity was given by the thermal velocity

$$U_v = (RT_p/2W_v)^{1/2} \quad (10)$$

where W_v is the molecular weight of the vapor. To calculate the density of vaporized gas ρ_v, the vapor pressure of the particle was estimated from the Clausius−Clapeyron equation. Since the chemical components of the vapor have not been identified in this present work, attempts to obtain the heat of the vaporization and the boiling point of the particles were carried out by fitting the temporal decays of the particle temperatures in Figure 5 with the numerical solutions of the differential equation (eq 3). The solid lines in Figure 5 are the simulated temporal decays of the particle temperatures with various surrounding media. It was found that the temporal decays of the particle temperatures were well simulated when the heat of vaporization was around 300 kcal mol^{-1} and the boiling point of the particles was around 3000 K. With these estimated values, the contribution of heat radiation, heat transfer to the surrounding gas, and particle vaporization was determined by calculating each term on the right-hand side of eq 3. The results are shown in Figure 8. The relative importance of the heat loss mechanism was plotted in a logarithmic form. As shown in Figure 8, the vaporization process decayed within 0.4 μs, which was consistent with the conclusions derived by the difference of the cooling rates between the different surrounding media. The heat radiations decayed faster than the heat conduction, but the decay rates of this process were much slower than those of the vaporization process.

By monitoring the temporal decays of the apparent particle temperatures with various surrounding media, the vaporization processes of the aerosol particles were suggested. Numerical simulations also suggested that the vaporization process played a key role within 0.4 μs after the irradiation of the 1064 nm

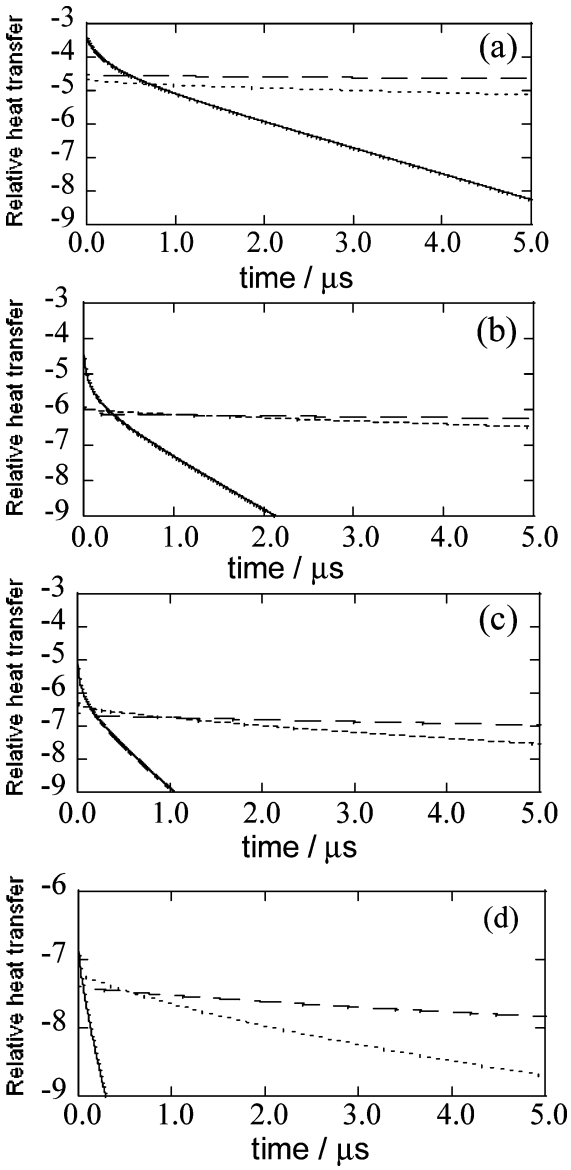

Figure 8. Comparison of the relative magnitudes of various heat loss mechanisms: (a) He; (b) Ar; (c) N_2; (d) CO_2. Solid lines, vaporization; dashed lines, heat conduction; dotted lines, heat radiation.

pulsed laser irradiation. However, since no emissions from Mo atoms were observed in Figure 4, more direct proof of the particle vaporization processes was desired. Since Mo atoms are known to emit atomic lines at 313 nm,[17] attempts to detect the emissions of Mo atoms in the incandescence spectra were carried out with a higher laser fluence of the fundamental light of the Nd:YAG laser at 1064 nm. Figure 9 shows the incandescence spectra obtained with a laser fluence of 340 mJ/cm^2. As shown in Figure 9, the atomic emissions of Mo atoms appeared around 310 nm in the spectra, which was direct proof for the vaporization process of the aerosol particles by the pulsed laser irradiation at 1064 nm. Other emission lines of Mo atoms were also detected around 380, 420, and 540 nm because of the higher particle temperature. However, all of the emission lines of Mo atoms disappeared within 350 ns after the pulsed irradiation at 1064 nm.

Fits to the experimental spectra with the Planck function (eq 2) were also carried out to obtain the apparent particle temperatures. As shown by the solid lines of Figure 9, although the simulated incandescence spectra were not in good agreement at shorter wavelengths, the incandescence spectra with higher

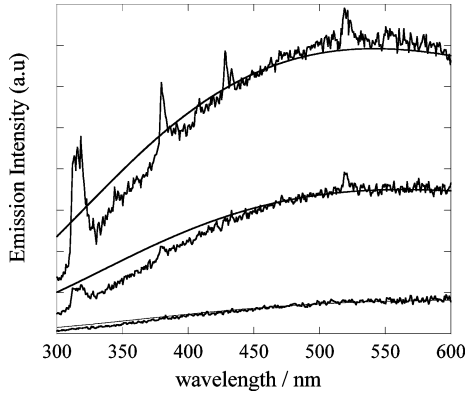

Figure 9. Laser-induced incandescence spectra of the laser-heated aerosol particles formed by the irradiations of the fourth harmonic of the Nd:YAG laser at 266 nm to the gaseous mixtures of 0.1 Torr of $Mo(CO)_6$ in 600 Torr of Ar gas. Each part corresponds to different delay times of (a) 50 ns, (b) 150 ns, and (c) 350 ns between the measurement and the pulsed irradiation of the fundamental light at 1064 nm with a fluence of 340 mJ/cm^2 for heating the aerosol particles in the reaction cell. The solid lines are the simulated spectra at apparent particle temperatures of (a) 5300 K, (b) 5100 K, and (c) 4700 K.

laser fluences were simulated with apparent particle temperatures of 5300, 5100, and 4700 K for delay times of 50, 150, and 350 ns, respectively. The boiling point of Mo metals is around 4800 K, and it is consistent that the atomic emissions appeared only with delay times of 50 and 150 ns. When the delay time between the pulsed laser irradiation at 1064 nm and the observation was 350 ns, the apparent particle temperature decreased below the boiling point of Mo metals and therefore the atomic emissions of Mo atoms disappeared. The observation that the maximum apparent particle temperature shown in Figure 5 was below the boiling point of Mo metals appeared to be inconsistent with the previous conclusions that the main cooling process up to 0.4 μs after the pulsed 1064 nm laser irradiations was the vaporization process only because there were no differences in the rates of the particle-cooling processes between the surrounding gases. However, the boiling points of the graphite were around 3370 K, which was lower than the maximum apparent particle temperatures irradiated by the fundamental light of the Nd:YAG laser, as shown in Figure 5. Therefore, the chemical components of the particles that vaporized during the delay times up to 0.4 μs in Figure 5 were possibly graphite. It is reasonable to assume that the particles contain not only Mo atoms but also carbon atoms as impurities because the particles were synthesized by the photolysis of $Mo(CO)_6$ in the gas phase. The other possible chemical components that vaporized during the delay times up to 0.4 μs in Figure 5 were the MoC phase formed by the photolysis of $Mo(CO)_6$ in the gas phase. Although the phase diagram of the molybdenum−carbon system was investigated by several researchers and six different phases have been identified in the molybdenum−carbon system,[21,22] the boiling point of this MoC phase has not been identified. According to Velikanova et al.,[21] the melting point of MoC phases is between 2200 and 2700 K, depending on the Mo-versus-carbon ratios. Therefore, the boiling point might possibly be around 3400 K like a graphite phase and hence the MoC phase could be the chemical components that vaporize by the irradiations of the pulsed 1064 nm laser light, as shown in Figure 5. Identification of the chemical components that vaporized by the laser irradiations will also give new insights for understanding the interactions between the aerosol particles of the multiple components and the pulsed laser beams.

Conclusion

The mechanism of the heat transfer processes of the aerosol particles was investigated by monitoring the incandescence spectra using an ICCD detector at various delay times after the pulsed laser heating using the fundamental light of a Nd:YAG laser at 1064 nm. By converting the incandescence spectra to the corresponding apparent particle temperatures using the Planck function, the cooling processes of the laser-heated particles were investigated. It was found that the vaporization processes were important up to 0.4 μs and after 0.4 μs the heat transfer to the surrounding media became important by comparing the cooling rates of the laser-heated particles between the different surrounding media. The vaporization process of the aerosol particles was evidenced by observing the emissions of the constituent molybdenum atoms with higher laser fluence of the fundamental light of the Nd:YAG laser at 1064 nm. The vaporization processes of the aerosol particles were found to affect the intensity of the laser-induced incandescence based on the relationships between the intensity of the laser-induced incandescence and the laser fluence at 1064 nm. The particle diameters formed by the photolysis of $Mo(CO)_6$ were larger in the order of He, Ar, N_2, and CO_2, which was elucidated from the calculation by the theory of heat conduction.

Acknowledgment. This work was partly supported by Showa Shell Sekiyu Foundation for Promotion of Environmental Research and by the Grant-in-Aid for Young Scientists (B) from the Ministry of Education, Culture, Sports, Science and Technology, Japan (No. 13750714), which is greatly appreciated.

References and Notes

(1) Chen, S.; Ingram, R. S.; Hostetler, M. J.; Pietron, J. J.; Murray, R. W.; Schaaff, T. G.; Khoury, J. T.; Alvarez, M. M.; Whetten, R. L. *Science* **1998**, *280*, 2098.
(2) Li, L.; Hu, J.; Yang, W.; Alivisatos, A. P. *Nano Lett.* **2001**, *1*, 349.
(3) Takami, A.; Yamada, H.; Nakano, K.; Koda, S. *Jpn. J. Appl. Phys.* **1996**, *35*, L781.
(4) Kurita, H.; Takami, A.; Koda, S. *Appl. Phys. Lett.* **1998**, *72*, 789.
(5) Takami, A.; Kurita, H.; Koda, S. *J. Phys. Chem. B* **1999**, *103*, 1226.
(6) Kamat, P. V.; Flumiani, M.; Hartland, G. V. *J. Phys. Chem. B* **1998**, *102*, 3123.
(7) Eckbreth, A. C. *J. Appl. Phys.* **1977**, *48*, 4473.
(8) Axelesson, B. A.; Collin, R.; Bengtsson, P. E. *Appl. Opt.* **2000**, *39*, 3683.
(9) Quay, R., Lee, T. W.; Ni, T.; Santoro, R. J. *Combust. Flame* **1994**, *97*, 384.
(10) Ni, T., Pinson, J. A.; Gupta, S.; Santoro, J. R. *Appl. Opt.* **1995**, *34*, 7083.
(11) Vander Wal, R. L. Presented at the Twenty-Sixth Symposium (International) on Combustion, The Combustion Institute, Pittsburgh, PA, 1996; p 2269.
(12) Melton, L. A. *Appl. Opt.* **1984**, *23*, 2201.
(13) Roth, P.; Filippov, A. V. *J. Aerosol Sci.* **1996**, *27*, 95.
(14) Filippov, A. V.; Markus, M. W.; Roth, P. *J. Aerosol Sci.* **1999**, *30*, 71.
(15) Schraml, S. W.; Bader, K.; Leipertz, A. *Appl. Opt.* **1998**, *37*, 5647.
(16) Vander Wal, R. L.; Ticich, M.; West, J. R. *Appl. Opt.* **1999**, *38*, 5867.
(17) Trushin, S. A.; Sugawara, K.; Takeo, H. *Chem. Phys. Lett.* **1995**, *236*, 402.
(18) Vander Wal, R. L.; Jensen, K. A. *Appl. Opt.* **1998**, *37*, 1607.
(19) Vander Wal, R. L.; Choi, M. Y. *Carbon* **1999**, *37*, 231.
(20) Forst, W. *Theory of Unimolecular Reactions*; Academic: New York, 1973. Gilbert, R. G.; Smith, S. C. *Theory of Unimolecular and Recombination Reactions*; Blackwell Science: Oxford, U.K., 1990. Holbrook, K. A.; Pilling M. J.; Robertson S. H. *Unimolecular Reaction Dynamics*; Oxford University Press: New York, 1996.
(21) Velikanova, Y. Ya.; Kublii, V. Z.; Khaenko, B. V. *Powder Metall. Met. Ceram.* **1988**, *27*, 891.
(22) Hugosson, H. W.; Eriksson, O.; Nordstrom, L.; Jasson, U.; Fast, L.; Delin, A.; Wills, J. M.; Johansson, B. *J. Appl. Phys.* **1999**, *86*, 3758.